

# Retrieval-Warmed Energy-Based Reasoning: A Five-Arm Ablation Methodology for Diffusion-as-Inference on Structured Reasoning Tasks

Libo Sun<sup>1</sup>, Po-Wei Harn<sup>2</sup>, Zewei Zhang<sup>1</sup>, Peixiong He<sup>1</sup>, Xiao Qin<sup>1,†</sup>

<sup>1</sup>Department of Computer Science and Software Engineering, Auburn University, Auburn, AL 36830, USA

<sup>2</sup>Department of Information Management, National Central University, Taoyuan 320317, Taiwan

<sup>†</sup>Corresponding author.

libo@auburn.edu, harnpowei@ncu.edu.tw, zez0001@auburn.edu, pzh0029@auburn.edu, xqin@auburn.edu

## Abstract

Warm-started diffusion samplers accelerate iterative inference, but it is rarely clear which part of the pipeline carries the gain. We study **retrieval-warmed energy-based reasoning (RW-EBR)** — an IRED energy-based diffusion model [Du *et al.*, 2024] augmented with a Modern Hopfield trajectory memory — and contribute a **five-arm ablation methodology** (oracle, best-constant, per-query-random, shuffled, aligned) that separates three confounded effects: class-prior bias shift, stochastic warm-starting, and graph-aligned value reuse. The diagnostic decomposition is adapted from LLM-RAG evaluation [Ru *et al.*, 2024]. On **connectivity-2** (Erdős-Rényi all-pairs reachability), the aligned-vs-shuffled-oracle swing reaches +35 **pp** balanced accuracy on a fixed 1,000-graph validation-set diagnostic, with value distribution and retrieval mechanics fixed, only per-graph alignment destroyed, while per-query random initialisation falls below cold — per-graph alignment, not bias shift or stochasticity, dominates. Yet the *deployable* cold-prediction pipeline misses the acceptance gate at stored-value quality. The same diagnostic logic, stopped at the key-quality screen, applied to **Sudoku** with a task-specific key encoder produces a clean negative at a *different* component — key quality, under the current setup. The decomposition names the first blocking component on each task. The setting — graph reachability refined by an iterative diffusion sampler, with explainability of failure modes as the lens — places the work within structured and spatio-temporal reasoning.

## 1 Introduction

Iterative inference procedures — diffusion samplers, energy-based reasoning models — are increasingly *warm-started*: rather than initialising from noise, the sampler is seeded with a candidate solution, often one retrieved from a memory of past solutions, to cut the number of refinement steps. When such a pipeline improves, or fails, it is rarely clear *which* part

is responsible. A warm-start can help because the retrieved content is genuinely task-relevant, because it shifts the initialisation toward a better region regardless of content, or simply because any per-query perturbation breaks a degenerate equilibrium. These explanations imply very different things about when retrieval warm-starting will generalise, yet a single end-to-end accuracy number cannot tell them apart. We frame this as explainable failure attribution for structured-reasoning systems: localising which component of a reasoning pipeline drives an outcome is a question of diagnostic evaluation, not of aggregate benchmark performance. The setting that grounds the study — relational structure (all-pairs reachability over an Erdős-Rényi graph) refined by an iterative diffusion sampler — is a graph- and iteration-shaped instance of structured and spatio-temporal reasoning.

We study this attribution problem in **retrieval-warmed energy-based reasoning (RW-EBR)**: an IRED energy-based diffusion model [Du *et al.*, 2024] augmented with a Modern Hopfield trajectory memory [Ramsauer *et al.*, 2021] that supplies a per-query warm-start. Our contribution is a **five-arm ablation methodology** — oracle, best-constant, per-query-random, shuffled, and aligned — that separates three confounded effects of a retrieval warm-start: class-prior bias shift, stochastic warm-starting, and graph-aligned value reuse. We organise the analysis with a three-component decomposition — key quality, warm-start mechanism, stored-value quality — adapting the retriever- and generator-side diagnostic logic of LLM-RAG evaluation [Ru *et al.*, 2024]. We claim neither the decomposition nor the partial-noise warm-start mechanism as novel — SDEdit [Meng *et al.*, 2022] is the mechanism’s predecessor, with WSD [Scholz and Turner, 2025] the closest learned-warm-start competitor. The contribution is the ablation methodology and its application to retrieval-warmed iterative inference, plus the two empirical findings it surfaces.

The **first finding** is an alignment effect on connectivity-2 (all-pairs reachability on Erdős-Rényi graphs). Under oracle memory, the swing between the aligned arm and the shuffled arm — gold values whose (key, value) pairings are permuted across queries, holding the value distribution and retrieval mechanics fixed — is +35 **pp** in balanced accuracy. A constant-init sweep bounds the bias-shift contribution to  $\leq +8$  pp, and per-query random initialisation lands at

−1.5 to −3.1 pp: per-graph alignment, not bias shift and not per-query stochasticity, is the dominant lever. These warm-start arms are run as a fixed validation-set diagnostic (1,000 graphs, seed 20260420); multi-seed warm-start replication is left for a larger study. The deployable cold-prediction pipeline nonetheless misses the −2 pp acceptance gate ( $\Delta\text{bal} = -4.09$  pp); the same decomposition localises that failure to stored-value quality.

The **second finding** is that the failure mode is heterogeneous. We apply the same diagnostic logic — contrastive key training and the quality-ratio gate, stopped at the key-quality screen — to Sudoku with a task-specific encoder, and obtain a clean negative at a *different* component: under the current mask-aware solved-board target and 500-candidate pool, the key encoder itself cannot clear its quality gate, whereas on connectivity the encoder passes and stored-value quality is the bottleneck. The two case studies show the three-component decomposition surfacing a different bottleneck on each task, rather than collapsing them into a single end-to-end number.

We wrap IRED as the base reasoning model and do not modify it: IRED’s sampler initialises from a Gaussian (its Algorithm 2 hard-codes  $\tilde{y} \sim \mathcal{N}(0, I)$ ). Our principled negatives concern the retrieval addition we study, not the IRED backbone.

In summary, we contribute (i) a five-arm ablation methodology for retrieval-warmed iterative inference, separating bias shift, stochastic warm-starting, and aligned value reuse; (ii) an aligned-vs-shuffled-oracle alignment effect on connectivity-2 that isolates per-graph value alignment as the dominant lever; and (iii) a heterogeneous-failure case study — under the same diagnostic workflow, connectivity-2 fails at stored-value quality and Sudoku at key quality — identifying the first blocking component on each task.

## 2 Methods

We evaluate on **connectivity-2** [Du *et al.*, 2024]: predict the all-pairs reachability matrix of an undirected Erdős–Rényi  $G(N=12, p=0.2)$  graph from its adjacency. Adjacency and targets are rescaled to  $\pm 1$ ; this is cell-level binary classification with positive (“path exists”) prior  $\approx 0.63$ . Training and evaluation both use IRED’s GraphConnectivityDataset. The base reasoning model (**G0**) is IRED’s 32-channel GraphEBM, trained for 30k steps under the IRED denoising objective (MSE on rescaled  $\pm 1$  targets) at 10 diffusion timesteps, with energy-landscape supervision and inner-loop optimisation enabled. A sample drawn at  $T$  inference timesteps from the unaugmented model is the **cold**  $T=T$  baseline.

Retrieval keys come from a 3-layer GIN [Xu *et al.*, 2019] with a **label-ordered readout** — per-node features concatenated in node-label order rather than sum-pooled — and a learned per-position id embedding on the layer-0 features. Label-ordered readout is engineering for our setting: sum-pool readouts are permutation-invariant, which would destroy the label-indexed structure the warm-start consumer needs, since retrieved reachability matrices must align with the query’s node labelling; the id embedding distinguishes

degree-symmetric collapse cases. The encoder is trained with a supervised contrastive loss [Khosla *et al.*, 2020] on the 4 target-nearest neighbours of each anchor at temperature  $\tau=0.1$  for 3,000 steps; the pair-similarity target is per-edge Hamming agreement of reachability. GIN and SupCon are off-the-shelf and the design choices are engineering, not a contribution; Section 4.1 reports the resulting key quality.

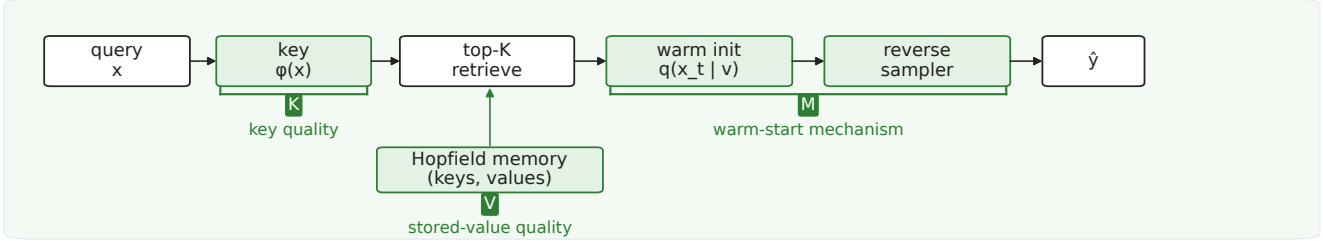
A capacity-10,000 Modern Hopfield trajectory memory [Ramsauer *et al.*, 2021] stores (key, value) pairs whose values are base-model trajectories, populated **write-once** during a warm-up phase by running cold inference at  $T_{\text{anchor}}=10$  over a random stream of 10,000 training examples; there are no eval-time writes. At eval time a query’s key retrieves a value via a  $\beta$ -temperature softmax over the top-8 cosine similarities, where the inverse temperature  $\beta$  controls retrieval peakedness, and the retrieved value seeds the IRED sampler in one of two ways. **Option A** replaces the  $t=0$  initialisation with the retrieved value and runs  $K_{\text{refine}}$  optimisation-step iterations. **Option B** — the primary reported path — forward-noises the retrieved value to an injection timestep  $t_{\text{inject}}$  via the standard diffusion forward marginal  $q(x_t | x_0)$ , then runs the reverse IRED `p_sample_loop` from  $t_{\text{inject}}$  down to 0. Reported runs use  $t_{\text{inject}}=2$  — a mild re-noising on the model’s 10-timestep diffusion schedule — with  $\beta=20$ ; Option A at  $K_{\text{refine}}=10$  is reported alongside it for robustness. Both reduce forward-pass count relative to a full cold sample.

All connectivity G0 and G1 runs share a fixed cached validation set of 1,000 graphs (seed 20260420). The headline metric is **balanced accuracy**  $= \frac{1}{2}(\text{rec}_+ + \text{rec}_-)$ , reported with raw accuracy and per-class recall; the  $\approx 63/37$  class imbalance makes raw accuracy a misleading gate, whereas balanced accuracy is immune to prior-collapse on either class. The **G1 acceptance gate** requires  $\Delta\text{bal\_acc}(\text{warm} - \text{cold}) \geq -2$  pp at a forward-pass speedup  $\geq 2\times$ . We use this gate as an *operational diagnostic screen* for the present study — a sanity threshold for when to stop reporting an arm as a candidate deployable warm-start, not a claim about external task-level success. The −2 pp tolerance is roughly  $15\times$  the per-seed cold noise floor (balanced-accuracy std 0.13 pp across 5 seeds; Section 4.3): any violation lies well outside per-seed sampling jitter, while still permitting a small accuracy drop when offset by the speedup. PASS/FAIL labels below refer to this internal screen.

We additionally exercise component K on Sudoku using the SATNet-style [Wang *et al.*, 2019] dataset from IRED [Du *et al.*, 2024]. The key encoder is a 3-layer ResNet ( $\sim 593$ k parameters) trained with the same SupCon objective for 3,000 steps; the per-anchor similarity target is per-cell argmax agreement restricted to query unknowns, scored against a 500-candidate in-batch pool. Pass criteria are  $\text{quality\_ratio} \geq 0.85$  and  $\text{ret\_top\_w}(\beta=20) \geq 0.30$ . The warm-start mechanism and stored-value components were not exercised on Sudoku; Section 5 reports the result.

**Reproducibility.** Upon publication we plan to release a supplementary archive containing training and evaluation scripts for the connectivity-2 G0 backbone, the contrastive key encoder, and all five G1 warm-start arms (cold, oracle, shuffled, best-constant, and per-query random), together with

### A. Retrieval-warmed inference pipeline



### B. Five ablation arms × three failure components

Arm	K <sub>key</sub>	M <sub>mechanism</sub>	V <sub>value</sub>	Diagnostic role
<i>aligned cold-pred</i>	✓	✓	✓	deployable reference
<i>aligned oracle</i>	✓	✓	★	V-quality upper bound
<i>shuffled oracle</i>	✓	✓	★×	K-V alignment break
<i>best constant</i>	∅	✓	C	bias-only warm start
<i>per-query random</i>	∅	✓	R	stochastic value control

✓ learned/real    ∅ bypassed retrieval    ★ oracle value    C constant value    ★× mis-keyed oracle value    R random value

Figure 1: **Diagnostic apparatus for retrieval-warmed inference.** (A) RW-EBR pipeline annotated with the three testable components: key quality (K), warm-start mechanism (M), stored-value quality (V). (B) Five-arm suite as a component matrix: ✓ = learned/real, ★ = oracle stored values, ★× = mis-keyed oracle, ∅ = bypassed task-informative retrieval, C/R = constant or random stored values.

their fixed configurations; the Sudoku key-encoder training script and SupCon configuration; the validation-set seed and the 5-seed cold noise-floor script; and the figure scripts producing all six figures of the paper. The archive reproduces all reported tables and figures against the cached validation set, and includes a unit-test suite covering the evaluation utilities.

## 3 Decomposing Retrieval-Warmed Inference

We decompose retrieval-warmed inference into three components that can fail independently: (K) **key quality** — does the encoder map inputs to keys whose retrieved values warm-start usefully? Measured by `quality_ratio`: the target similarity between a query and its top-1 retrieved candidate, divided by the best target similarity available among all candidates; (M) **warm-start mechanism** — given a retrieved value of fixed quality, does the inference loop refine it toward the true target? Isolated by an **oracle-memory ablation** writing ground-truth values directly to memory; (V) **stored-value quality** — does the cold model produce predictions useful as future warm-starts? This adapts LLM-RAG diagnostic decompositions [Ru *et al.*, 2024; Sivakumar *et al.*, 2026] to retrieval-warmed *iterative* inference. Figure 1 summarises the apparatus and the five arms.

arm / config	bal	$r_+$	$r_-$	spd	$\Delta\text{bal}$
<i>Sanity arm — deployable cold-pred memory:</i>					
cold ( $T=10$ )	.755	1.000	.511	1.0×	—
<b>warm, cold-pred Opt B</b>	<b>.715</b>	.999	<b>.430</b>	3.3×	-4.09
<i>Oracle arm — ground-truth memory:</i>					
cold ( $T=10$ )	.753	1.000	.505	1.0×	—
<b>warm, oracle Opt B</b>	<b>.977</b>	.993	<b>.960</b>	3.3×	+22.39
<b>warm, oracle Opt A</b>	.957	.989	.926	5.5×	+20.45

Table 1: Warm-start arms on connectivity-2 ( $\beta=20$ ; Opt B at  $t_{\text{inj}}=2$ , Opt A at  $K_{\text{ref}}=10$ ). Sanity arm: deployable cold-pred memory misses the gate at stored-value quality (V FAIL). Oracle arm: both warm-start variants clear it (M PASS). Within-arm  $\Delta\text{bal}$  vs each arm’s own cold reference. Fixed  $n=1,000$  validation set; multi-seed caveat in §4.5.

## 4 Connectivity-2: A Stored-Value-Quality Failure

We walk the three components in turn on connectivity-2: the key encoder (Section 4.1), the warm-start mechanism (Section 4.2), and stored-value quality (Section 4.3). The five-arm ablation suite then decomposes the oracle result (Section 4.4), and two further interventions characterise the failure (Section 4.5).

## 4.1 Key Quality

Validation `quality_ratio` saturates at  $\approx 0.95$  (`gt_pred_top1`  $\approx 0.83$ , `gt_best`  $\approx 0.88$ ); `ret_top_w`( $\beta=20$ ) — the peakedness of softmax retrieval weights — reaches 0.49 against the  $1/8 = 0.125$  uniform floor (a prior MLP+MSE baseline plateaued at 0.40). The encoder passes the targeted relabeled-isomorph regression test — two labelings of a 4-node perfect matching that share all-degree-1 nodes yet whose reachability matrices agree on only 50% of cells; we do not claim universal isomorph discrimination. **Component K: PASS.**

## 4.2 Warm-Start Mechanism

The oracle ablation replaces cold-prediction memory writes with ground-truth reachability writes. This is non-deployable — we do not have ground truth at memory-write time in practice — but it measures what the inference mechanism achieves in this finite-memory setting given perfect stored values. The result is not a global upper bound; finite memory coverage, retrieval mismatch on the held-out validation set, top- $K$  averaging, and sampler stochasticity all remain potential limits even in the oracle condition. We report both warm-start variants from Methods: **Option B** at  $t_{\text{inject}}=2$  and **Option A** at  $K_{\text{refine}}=10$ . The two paths are independent —  $K_{\text{refine}}$  does not appear in Option B,  $t_{\text{inject}}$  does not appear in Option A.

Two observations follow from Table 1’s oracle arm. First, the **load-bearing lift is in `rec_-`**: it moves from 0.505 (chance) cold to 0.960 under Option-B warm inference with ground-truth memory; `rec_+` stays at  $\approx 0.99$ . The mechanism is correcting the negative class, not inflating accuracy via prior collapse. Second, both variants beat the  $2\times$  speedup gate ( $3.3\times$  Option B,  $5.5\times$  Option A) at near-saturated balanced accuracy.

A  $\beta$  sweep ( $\beta \in \{20, 40, 80, 160\}$ ), both variants — eight oracle cells total) passes the gate by  $\geq +18.91$  pp in every case. Notable: with oracle memory, *lower*  $\beta$  slightly outperforms higher  $\beta$  (Option B  $\Delta_{\text{bal}}$  at  $\beta=20$ :  $+22.39$  pp; at  $\beta=160$ :  $+20.75$  pp), inverting the cold-pred-memory trend (Section 4.3). Interpretation: high-quality stored values benefit from top- $K$  averaging that smooths cell-level disagreement between near-correct neighbours; low-quality stored values prefer peaky  $\beta$  to concentrate on the least-bad neighbour. **Optimal  $\beta$  depends on memory quality, not an architectural constant. Component M: PASS.**

## 4.3 Stored-Value Quality

Replacing oracle memory writes with cold-prediction memory writes is the only change from Section 4.2 — same key encoder, warm-start dispatch, retrieval temperature, and validation set. Both warm arms come from the same run so the comparison is direct; the two cold rows reflect within-run sampling jitter ( $\approx 0.3$  pp here; the cold noise floor measured separately across 5 seeds is balanced accuracy std 0.13 pp). All  $\Delta$ s reported here and in Section 4.4 dominate the noise floor by  $\geq 11\times$  (smallest, per-query uniform) to  $\geq 170\times$  (oracle).

The cold-pred warm row (Table 1, sanity arm) misses the  $-2$  pp gate by 2.09 pp. More informatively, `rec_-` **gets worse**,

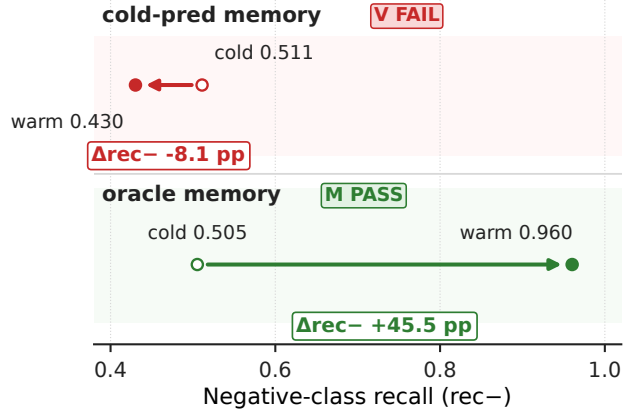


Figure 2: **Negative-class recall carries the connectivity-2 story** (Option B,  $t_{\text{inject}}=2$ ,  $\beta=20$ ). Cold-prediction memory *degrades* `rec_-` under warm-start (0.511  $\rightarrow$  0.430); oracle memory recovers it sharply (0.505  $\rightarrow$  0.960). `rec_+` stays near 1.0 throughout.

comparison	Option B	Option A
oracle aligned vs. cold	+22.39	+20.45
best constant vs. cold	+7.92	+5.65
per-query uniform $[-1, 1]$ vs. cold	-1.54	-10.25
per-query $\mathcal{N}(0, 1)$ vs. cold	-3.09	-10.46
shuffled oracle vs. cold	-12.80	-14.30
<b>aligned – best constant</b>	<b>+14.47</b>	<b>+14.80</b>
<b>aligned – shuffled</b>	<b>+35.19</b>	<b>+34.75</b>

Table 2: Decomposition of the oracle lift,  $\Delta_{\text{bal}}$  in pp at  $\beta=20$ . Best constant:  $c=-0.25$  (Option B),  $c=-0.75$  (Option A).

**not better**: 0.511 cold  $\rightarrow$  0.430 warm in the same arm (Figure 2). The warm path inherits and amplifies the cold model’s class bias rather than failing to fix it; retrieval finds high-similarity neighbours (key quality is fine), but every neighbour’s stored prediction is itself biased toward the positive class.

The oracle/cold-pred gap ( $\Delta_{\text{bal}} = +22.39$  pp vs  $-4.09$  pp within the same run) is the cleanest component-attribution evidence we have: 26.5 pp of balanced accuracy separates *identical* mechanism and retrieval, differing only in stored-value quality. An independent earlier run reproduces the cold-pred result at  $\Delta_{\text{bal}} = -3.75$  pp on a different cold draw, qualitatively similar (both miss the  $-2$  pp gate by comparable margins). By the decomposition of Section 3, the mechanism and retrieval components are not the bottleneck on this task; the stored-value component is. **Component V: FAIL.**

## 4.4 Bias Shift Versus Alignment: The Five-Arm Suite

Sections 4.2 and 4.3 contrasted the oracle mechanism’s  $+22$  pp gain with the deployable pipeline’s failure. We now scrutinise the oracle lift itself: is it genuine per-graph value reuse, or class-prior shift alone? Equivalently: would any sufficiently-negative warm init achieve a similar lift by break-

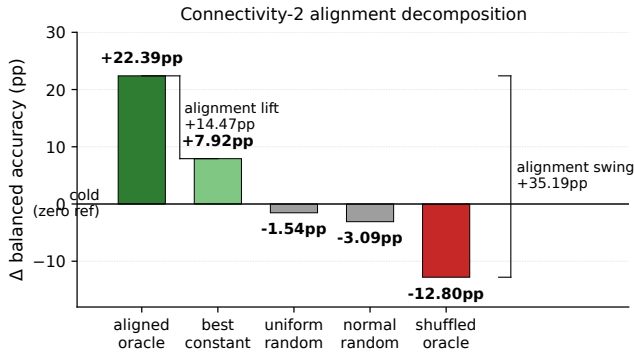


Figure 3: **Alignment decomposition on connectivity-2** (Option B,  $t_{\text{inject}}=2$ ,  $\beta=20$ ). The aligned oracle exceeds the best bias-only warm-init by +14.47 pp and a shuffled oracle (same gold values, (key, value) pairings permuted across queries) by +35.19 pp, isolating per-graph alignment as the dominant lever. Per-arm  $\Delta\text{bal}$  in Table 2.

ing the cold model’s positive-bias equilibrium, with retrieval contributing nothing? Three ablations decompose it: a constant warm-init sweep  $c \in \{-1, \dots, 1\}$ ; a **shuffled-oracle** arm (gold values, but with (key, value) pairings permuted across queries — preserving the value distribution while destroying per-graph alignment); and a **per-query stochastic init** arm (self-retrieve with per-entry random storage at  $\beta=20$ ,  $t_{\text{inject}}=2$ ; uniform  $[-1, 1]$  and  $\mathcal{N}(0, 1)$ ).

The constant sweep stores a constant tensor of value  $c$  at every memory slot; retrieval over identical values is a no-op, so the warm-start receives exactly  $c$ . The per-query stochastic arms use self-retrieve with per-entry random storage — top-1 self-similarity dominates the softmax (mean retrieval-top weight 0.887), so each query retrieves predominantly its own pre-stored random vector. Table 2 and Figure 3 report the results.

The decomposition tells a consistent story. Bias shift is bounded: no constant warm init exceeds +8 pp  $\Delta\text{bal}$ . On top of that best bias-only baseline, aligned ground-truth retrieval adds +14.5 pp, and the two warm-start variants — which consume the init differently — agree on this gap to within 0.4 pp. Misalignment does not merely fail to help but actively poisons: the shuffled oracle falls  $\approx 20$  pp *below* the best constant, so alignment is a dominant, non-additive lever rather than a small perturbation. And per-query stochasticity is not the missing axis — both random-init arms fall at or below cold under Option B.

We state the contribution precisely. That lift is the *aligned-vs-best-constant* gap, not a one-sided “retrieval contributes +14.5 pp” claim; the full alignment effect is the +35 pp swing from misaligned to aligned ground truth. A tuned constant prior delivers up to +8 pp; the remaining lift requires per-graph alignment between key and stored value, which contributes nearly twice what the best bias shift does. The objection that the oracle merely supplies a better class prior or a generic warm-init regulariser does not survive these controls.

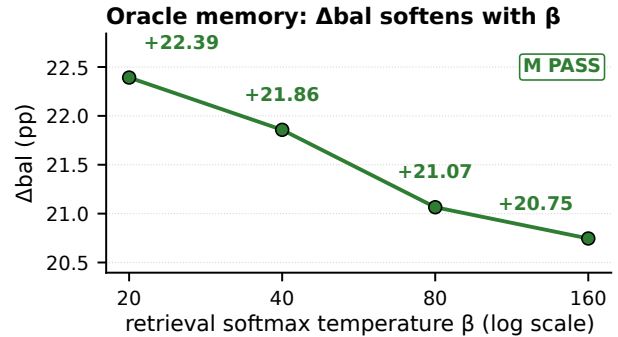
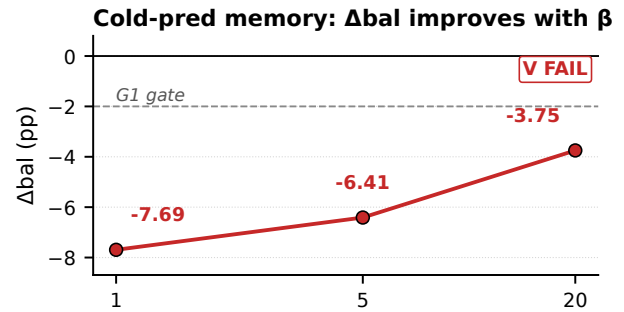


Figure 4:  **$\beta$ -trend inversion:  $\Delta\text{bal}$ ’s response to  $\beta$  depends on stored-value quality** (Option B,  $t_{\text{inject}}=2$ ). Cold-prediction memory:  $\Delta\text{bal}$  improves monotonically with  $\beta$  but never clears the  $-2$  pp gate. Oracle memory: trend inverts — highest at the lowest  $\beta$  tested, softening as  $\beta$  grows. Non-overlapping  $\beta$ -grids; diagnostic trends, not a head-to-head sweep.

#### 4.5 Why Stored-Value Quality Fails

Two interventions further characterise the failure as representational rather than procedural.

**Threshold tuning.** Cold raw outputs lie in  $[-0.99, +0.99]$  and are evaluated at threshold  $\tau=0$ . Sweeping  $\tau \in [-1, 1]$  in steps of 0.02 over the validation set and selecting  $\tau$  for balanced accuracy yields a maximum lift of +0.47 pp (at  $\tau=+0.96$ : acc 0.821, bal. acc 0.760,  $\text{rec}_+$  1.000,  $\text{rec}_-$  0.520, against  $\tau=0$ : 0.817, 0.755, 1.000, 0.511), small relative to the  $-2$  pp gate and not qualitatively corrective. Crucially,  $\text{rec}_+$  stays at 1.000 up to  $\tau=+0.96$  — the model does not even consider assigning negative class until the threshold reaches 96% of its prediction range. Threshold shifting reveals no recoverable balanced-accuracy fix under this probe; features are sharply committed and largely class-biased. The “right features, wrong decision boundary” diagnosis is not supported.

**Class-weighted retraining.** A more invasive intervention: modify IRED’s denoising MSE to apply a  $4\times$  per-cell weight on negative-class cells, by subclassing the IRED denoising objective with a per-cell loss weight applied inside the diffusion loss, mirroring the existing per-cell weighting precedent in IRED’s shortest-path task. After 30,000 steps under the same schedule, balanced accuracy *decreased* by 3.2 pp: the original G0 reaches bal. acc 0.755 ( $\text{rec}_+$  1.000,  $\text{rec}_-$  0.511 — strongly biased toward the positive class), while the re-

metric	gate	best (step)	step 3000
quality_ratio	$\geq 0.85$	0.434 (2000)	0.420
ret_top_w( $\beta=20$ )	$\geq 0.30$	0.242 (3000)	0.242
recall@1	diagnostic	0.010 (1500)	0.006
loss EMA	( $\approx 4.16$ )	—	5.290

Table 3: Sudoku key-encoder training (3000 SupCon steps). Both key-quality kill criteria fail by margin, and validation metrics plateau despite continued loss descent; we stop before evaluating M/V.

balanced G0 reaches 0.724 (rec<sub>+</sub> 0.447, rec<sub>-</sub> 1.000 — flips toward the negative class). The retrained model did not find a balanced equilibrium; it flipped polarity. Two degenerate equilibria with no balanced middle suggest the learned representation does not support balanced classification under the tested training recipe — class weighting decides only which side training collapses to.

The two probes converge on the same conclusion: the stored-value limit is consistent with a learned-representation limit under this training recipe rather than with a tunable boundary or loss weight. Two interventions that *should* have helped if the failure were only a decision-threshold or class-weighting artifact both fail to. The  $\beta$ -trend inversion of Figure 4 is the same story read through retrieval temperature: the direction of the trend depends on stored-value quality.

Several questions remain open. We have not shown that a larger or differently-architected G0 — a deeper GNN, an attention-based variant, an alternative loss — could not solve connectivity-2, nor that the oracle ceiling generalises to tasks where the cold model is already strong. By extension we expect iterative refill of warm predictions into memory to amplify cold bias, but we have not tested this formally. Our reverse path is the stochastic DDPM `p_sample`; whether a deterministic-reverse DDIM path behaves identically is untested — Option B covers the forward-init half, not the reverse. Finally, the warm-start ablations run on a single fixed validation set, and multi-seed warm-start replication is left for a larger study.

## 5 Sudoku: A Key-Quality Failure

Applying the same diagnostic logic to Sudoku — stopped at the key-quality screen, before the warm-start mechanism and stored-value components are exercised — produces a clean negative at a *different* component than connectivity. The ResNet key encoder (Methods) trained 3,000 steps reaches `quality_ratio` 0.42 (gate  $\geq 0.85$ , missed by half) and `ret_top_w( $\beta=20$ )` 0.242 (gate  $\geq 0.30$ , missed by 0.058 absolute); both metrics plateau (Table 3). Loss descends but validation metrics decouple after step 1500; we do not proceed to warm-start diagnostics under this setup.

The Hamming-similarity distribution on solved boards (Figure 6B) is unimodal at the iid baseline (mean =  $1/9 \approx 0.111$ ; q95 = 0.185, max = 0.395). `gt_best` — the in-batch maximum target similarity per anchor under the mask-aware target across 500 candidates — plateaus at  $\approx 0.30$  across all training checkpoints. Even with a perfect encoder, only  $\approx 30\%$  of the query’s unknown cells would match the true digit — a weak warm-start target relative to the cold end-

point’s 0.97 cell accuracy. The downstream warm-start effect is not measured here: Sudoku stops at the K-screen, before M/V are exercised.

Two distinct limits hold under the current setup. The encoder under-retrieves: `quality_ratio` 0.42 means top-1 retrievals reach less than half the in-batch best available similarity, so the encoder retrieves substantially worse than the candidate pool allows. Separately, the in-batch best itself plateaus at `gt_best`  $\approx 0.30$  — a candidate-pool / target ceiling, not an encoder verdict, so even a perfect retriever delivers warm-starts at only  $\approx 0.30$  absolute target similarity to the query. A better encoder alone could in principle clear the normalized `quality_ratio` gate; producing a useful warm-start signal on Sudoku, however, requires moving both limits. Sudoku fails at component K (key quality, under the current setup); connectivity fails at component V (stored-value quality, with the mechanism working) — Figure 5. A symmetry-aware encoder, a canonicalised or larger candidate pool, or a different value target could move these limits; we did not run those configurations.

## 6 Related Work

RW-EBR wraps IRED [Du *et al.*, 2024], whose energy-based diffusion solves the connectivity-2 and Sudoku tasks studied here; IRED’s ablations cover gradient-on-energy, multi-step refinement, and contrastive shaping — not memory or warm-start initialisation. IREM [Du *et al.*, 2022] is the earlier energy-minimisation ancestor, also without memory or warm-start. The warm-start step itself — forward-noise a retrieved value to  $t_{\text{inject}}$ , then denoise from  $t_{\text{inject}}$  down to 0 — is the standard partial-noise warm-start introduced by SDEdit [Meng *et al.*, 2022] for image editing; the forward step is the standard diffusion marginal  $q(x_t | x_0)$  shared by DDPM [Ho *et al.*, 2020] and DDIM [Song *et al.*, 2021], with DDIM distinguished by its deterministic reverse sampler (we use the stochastic DDPM `p_sample`). The closest learned-warm-start competitor is WSD [Scholz and Turner, 2025], which learns a per-query informed Gaussian prior for conditional generation. Sampler-distillation approaches such as Consistency Models [Song *et al.*, 2023] are a complementary acceleration axis (few-step approximation rather than warm-start init), not exercised here.

RDM [Blattmann *et al.*, 2022] and kNN-Diffusion [Sheynin *et al.*, 2022] condition image diffusion models on retrieved nearest neighbours; MEMENTO [Chalumeau *et al.*, 2025] conditions a combinatorial-optimisation solver on a memory bank. In all of these the retrieved item enters as a conditioning signal alongside the input; RW-EBR differs in the role of retrieval, where the retrieved vector is the warm-start initialisation of the sampler’s dynamical update rather than a conditioning vector. The trajectory memory itself is a Modern Hopfield network [Ramsauer *et al.*, 2021]; a recent theoretical line [Ambrogioni, 2024; Pham *et al.*, 2025] bridges diffusion models and associative memory, which we use operationally — retrieve a candidate trajectory and feed it as a warm-start — rather than developing it theoretically.

RAGChecker [Ru *et al.*, 2024] and RAG-X [Sivakumar *et al.*, 2026] decompose LLM retrieval-augmented-generation

	<b>K</b> Key quality encoder retrieval	<b>M</b> Mechanism oracle memory	<b>V</b> Stored values cold-pred memory
<b>Connectivity-2</b> G(12, 0.2) reachability	<b>quality_ratio <math>\approx 0.95</math></b> GIN + SupCon label-ordered readout ✓ <b>PASS</b>	<b><math>\Delta\text{bal} = +22.39\text{pp}</math></b> oracle ablation (Option B, $t_{\text{inject}}=2$ , $\beta=20$ ) ✓ <b>PASS</b>	<b><math>\Delta\text{bal} = -4.09\text{pp}</math></b> cold-pred memory; gate $\geq -2\text{pp}$ ✗ <b>FAIL · bottleneck</b>
<b>Sudoku</b> Sudoku 9x9 current setup	<b>quality_ratio <math>\approx 0.42</math></b> gate $\geq 0.85$ gt_best $\approx 0.30$ cap (500 cand) ✗ <b>FAIL · bottleneck</b>	<b>(not run)</b> STOP at component 1 - <b>not evaluated</b>	<b>(not run)</b> STOP at component 1 - <b>not evaluated</b>

✓ passes gate      ✗ misses gate      - stopped after earlier failure

Figure 5: **Heterogeneous failure modes across two reasoning tasks** (connectivity rows: Option B,  $t_{\text{inject}}=2$ ,  $\beta=20$ ; Sudoku: key-quality screen only). On connectivity-2, K and oracle M pass; the deployable cold-pred pipeline then fails at V ( $-4.09$  pp vs the  $-2$  pp gate). On Sudoku, the encoder itself blocks at K ( $\text{quality\_ratio} \approx 0.42$  vs the  $\geq 0.85$  gate,  $\text{gt\_best} \approx 0.30$  candidate-pool ceiling).

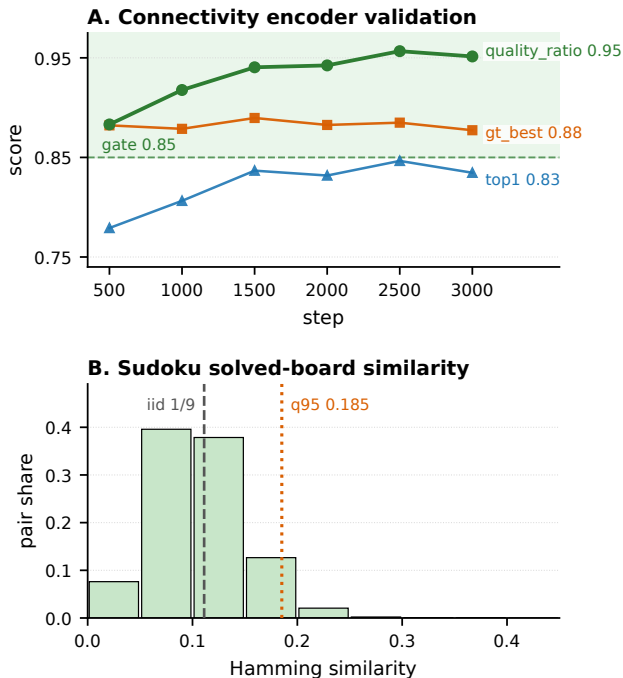


Figure 6: (A) Connectivity-2 encoder validation:  $\text{quality\_ratio}$  clears the  $\geq 0.85$  gate by step 500, saturating near 0.95 against the per-batch  $\text{gt\_best} \approx 0.88$  ceiling. (B) Sudoku solved-board Hamming similarity (999,000 pairs): unimodal at iid  $1/9$ ,  $q95 = 0.185$ ,  $\text{gt\_best} \approx 0.30$  — the candidate-pool side of Sudoku’s K-screen failure (see Section 5 for the encoder-side limit).

pipelines into retriever- and generator-side diagnostic metrics for failure attribution. Our three-component decomposition (key quality / warm-start mechanism / stored-value quality) adapts this logic to retrieval-warmed *iterative inference*; we do not claim the decomposition, the partial-noise warm-start mechanism, or the oracle-memory upper bound as novel primitives. The slot that differs from the LLM-RAG setting

is the warm-start mechanism — the retrieved vector enters a dynamical update, not a context window. What is distinctive across these prior threads is the application: we are not aware of any that tests its warm-start against a constant baseline, a per-query random control, and a shuffled-oracle arm, or that reports a component-level decomposition across two reasoning tasks under iterative inference.

## 7 Conclusion

We introduced a five-arm ablation methodology — oracle, best-constant, per-query-random, shuffled, and aligned — for attributing the behaviour of retrieval-warmed iterative inference. The full suite is exercised on connectivity-2 through an IRED energy-based diffusion backbone augmented with a Modern Hopfield trajectory memory; the same diagnostic logic is applied to Sudoku as a key-quality screen. On connectivity-2 the suite isolates per-graph key-value alignment as the dominant lever: a  $+35$  pp aligned-vs-shuffled-oracle swing that a tuned constant prior and per-query stochastic initialisation together cannot explain. The same decomposition identifies the first blocking component of the deployable pipeline on each task: stored-value quality on connectivity-2, key quality on Sudoku under the current setup. The oracle arms are diagnostic upper bounds, not deployable results; their value is in attribution. Coverage beyond these two tasks remains future work. Where a single end-to-end accuracy number reports only that retrieval warm-starting helped or failed, the methodology names the component — key quality, warm-start mechanism, or stored-value quality — that carried it: a localised verdict no aggregate score can give.

## References

- [Ambrogioni, 2024] Luca Ambrogioni. In search of dispersed memories: Generative diffusion models are associative memory networks. *Entropy*, 26(5):381, 2024.
- [Blattmann *et al.*, 2022] Andreas Blattmann, Robin Rombach, Kaan Oktay, Jonas Müller, and Björn Ommer. Semi-

- parametric neural image synthesis. In *Advances in Neural Information Processing Systems (NeurIPS)*, 2022.
- [Chalumeau *et al.*, 2025] Felix Chalumeau, Refiloe Shabe, Noah De Nicola, Arnú Pretorius, Thomas D. Barrett, and Nathan Grinsztajn. Memory-enhanced neural solvers for routing problems. In *Advances in Neural Information Processing Systems (NeurIPS)*, 2025.
- [Du *et al.*, 2022] Yilun Du, Shuang Li, Joshua B. Tenenbaum, and Igor Mordatch. Learning iterative reasoning through energy minimization. In *Proceedings of the 39th International Conference on Machine Learning (ICML)*, 2022.
- [Du *et al.*, 2024] Yilun Du, Jiayuan Mao, and Joshua B. Tenenbaum. Learning iterative reasoning through energy diffusion. In *Proceedings of the 41st International Conference on Machine Learning (ICML)*, 2024.
- [Ho *et al.*, 2020] Jonathan Ho, Ajay Jain, and Pieter Abbeel. Denoising diffusion probabilistic models. In *Advances in Neural Information Processing Systems (NeurIPS)*, 2020.
- [Khosla *et al.*, 2020] Prannay Khosla, Piotr Teterwak, Chen Wang, Aaron Sarna, Yonglong Tian, Phillip Isola, Aaron Maschiot, Ce Liu, and Dilip Krishnan. Supervised contrastive learning. In *Advances in Neural Information Processing Systems (NeurIPS)*, 2020.
- [Meng *et al.*, 2022] Chenlin Meng, Yutong He, Yang Song, Jiaming Song, Jiajun Wu, Jun-Yan Zhu, and Stefano Ermon. SDEdit: Guided image synthesis and editing with stochastic differential equations. In *International Conference on Learning Representations (ICLR)*, 2022.
- [Pham *et al.*, 2025] Bao Pham, Gabriel Raya, Matteo Negri, Mohammed J. Zaki, Luca Ambrogioni, and Dmitry Krotov. Memorization to generalization: Emergence of diffusion models from associative memory, 2025.
- [Ramsauer *et al.*, 2021] Hubert Ramsauer, Bernhard Schöfl, Johannes Lehner, Philipp Seidl, Michael Widrich, Thomas Adler, Lukas Gruber, Markus Holzleitner, Milena Pavlović, Geir Kjetil Sandve, Victor Greiff, David Kreil, Michael Kopp, Günter Klambauer, Johannes Brandstetter, and Sepp Hochreiter. Hopfield networks is all you need. In *International Conference on Learning Representations (ICLR)*, 2021.
- [Ru *et al.*, 2024] Dongyu Ru, Lin Qiu, Xiangkun Hu, Tianhang Zhang, Peng Shi, Shuaichen Chang, Cheng Jiayang, Cunxiang Wang, Shichao Sun, Huanyu Li, Zizhao Zhang, Binjie Wang, Jiarong Jiang, Tong He, Zhiguo Wang, Pengfei Liu, Yue Zhang, and Zheng Zhang. RAGChecker: A fine-grained framework for diagnosing retrieval-augmented generation. In *Advances in Neural Information Processing Systems (NeurIPS) Datasets and Benchmarks Track*, 2024.
- [Scholz and Turner, 2025] Jonas Scholz and Richard E. Turner. Warm starts accelerate conditional diffusion, 2025.
- [Sheynin *et al.*, 2022] Shelly Sheynin, Oron Ashual, Adam Polyak, Uriel Singer, Oran Gafni, Eliya Nachmani, and Yaniv Taigman. KNN-Diffusion: Image generation via large-scale retrieval, 2022.
- [Sivakumar *et al.*, 2026] Aswini Sivakumar, Vijayan Sugumar, and Yao Qiang. RAG-X: Systematic diagnosis of retrieval-augmented generation for medical question answering, 2026.
- [Song *et al.*, 2021] Jiaming Song, Chenlin Meng, and Stefano Ermon. Denoising diffusion implicit models. In *International Conference on Learning Representations (ICLR)*, 2021.
- [Song *et al.*, 2023] Yang Song, Prafulla Dhariwal, Mark Chen, and Ilya Sutskever. Consistency models. In *Proceedings of the 40th International Conference on Machine Learning (ICML)*, 2023.
- [Wang *et al.*, 2019] Po-Wei Wang, Priya L. Donti, Bryan Wilder, and J. Zico Kolter. SATNet: Bridging deep learning and logical reasoning using a differentiable satisfiability solver. In *Proceedings of the 36th International Conference on Machine Learning (ICML)*, 2019.
- [Xu *et al.*, 2019] Keyulu Xu, Weihua Hu, Jure Leskovec, and Stefanie Jegelka. How powerful are graph neural networks? In *International Conference on Learning Representations (ICLR)*, 2019.